2015 IEEE/RSJ International Conference on Intelligent Robots and Systems (IROS)
Congress Center Hamburg
Sept 28 - Oct 2, 2015. Hamburg, Germany

Extended Bicycle Model for Needle Steering in Soft Tissue

Bita Fallahi[1], Mohsen Khadem[1], Carlos Rossa [1], Ronald Sloboda [2], Nawaid Usmani [2], and Mahdi Tavakoli [1]

Abstract— **This paper represents an extension to the kinematic bicycle model for beveled-tip needle motion in soft tissue, which accounts for non-constant curvature paths for the needle tip. For a tissue that is not stiff relative to the needle, the tissue deformation caused by needle insertion deviates the needle tip position from a constant curvature path. The proposed model is obtained by replacing the bicycle wheels with omni-directional wheels that move in two orthogonal directions independently. Such wheels can move sideways, providing a means for modeling the deviations of the needle tip from a constant curvature path by incorporating new parameters in the model. Using an experimental setup, the needle is inserted into soft phantom tissue at different constant velocities and model parameters are fitted to experimental data. The model is verified by comparing the results from the model to empirical data.**

I. Introduction

Needle insertion is an effective technique used in minimally invasive procedures such as brachytherapy, biopsies and neurosurgery for diagnosis, delivery of treatments or sample removal. The efficiency of these methods is highly dependent on the accurate control and positioning of the needle tip since poor needle placement can cause undesirable side effects on neighboring tissues or organs. In order to improve the accuracy of the procedure, intelligent assistant robots can be employed to compensate for the targeting errors caused by needle deflection and tissue deformation. To this end, physical modelling of needle-tissue interaction provides a means to estimate needle deflection and provides an opportunity to minimize needle placement errors.

Several needle-tissue interaction models have been developed. This includes energy-based methods [1], [2], finite elements modelling [3], [4], [5], and flexible beam modelling [6], [7]. A Kinematic nonholonomic model has been proposed as an empirical parameter-identifiable model that can estimate needle deflection based only on limited knowledge about tissue-needle interaction. This model describes the kinematics of the needle tip based on constraints imposed by tissue and has been widely used for path planning and needle steering [8], [9], [10]. The main assumption made in this model is that the tissue is stiff relative to needle. Inserting the needle into stiff tissue causes negligible deformation in tissue as the needle bends. Thus, it is assumed that the needle tip moves on a circular path with a constant curvature. Approximating the path followed by the needle tip with a circle makes the path planing procedure simple as the radius and center of the circular path can be analytically derived. However, if the tissue is not stiff relative to the needle, as the needle bends during insertion the tissue is compressed and in turn displaces the needle tip from a constant curvature circle, thus producing non-circular paths [11], [1]. Ignoring the tissue motion may lead to inaccurate path planning and control of needle steering in soft tissue.

In this paper, we propose an extension to the kinematic bicycle model that will account for needle tip deflection with non-constant curvature. Using experimental data from needle insertion into different phantom tissues, we show that the radius of curvature of the needle tip path is influenced by the tissue stiffness. The kinematic bicycle model is modified to have new parameters enabling one to account for path variations caused by tissue deformation. Experimental validation of the extended model is reported for different needle-tissue combinations.

This paper is organized as follow. Section II presents a brief review of the bicycle model and its 3-DOF formulation for needle steering. In Section III the proposed extended bicycle model is presented and modifications made to the bicycle model are presented. In Section IV, the proposed model is experimentally validated and the results are compared to the bicycle model's results.

II. Background

A. General Bicycle Model

The kinematics of a bicycle moving in the $y-z$ plane is shown in Figure 1. The fixed frame and the body moving frame are denoted by $\{A\}$ and $\{B\}$, respectively. The origin of the moving frame is attached to the body at point P, somewhere between the two wheels. The posture of the body with respect to the fixed frame $\{A\}$ is described by the Cartesian position of point P and the rotation angle θ of frame $\{B\}$. The position and orientation of the wheels in the moving frame are characterized by $\ell_i (i = f, b)$ being the distances between the front and back wheels and point P, and $\beta_i (i = f, b)$ being the orientations of the wheels with respect to body frame $\{B\}$. For the general bicycle shown

This work was supported by the Natural Sciences and Engineering Research Council (NSERC) of Canada under grant CHRP 446520, the Canadian Institutes of Health Research (CIHR) under grant CPG 127768, and by the Alberta Innovates - Health Solutions (AIHS) under grant CRIO 201201232.

[1]B. Fallahi, M. Khadem, C. Rossa, PhD, and M. Tavakoli (Corresponding Author), PhD, are with the Department of Electrical and Computer Engineering, University of Alberta, Edmonton, Canada T6G 2V4. E-mail: {fallahi, mohsen.khadem, rossa, madhi.tavakoli}@ualberta.ca

[2]R. Sloboda and N. Usmani are with the Cross Cancer Institute and the Department of Oncology, University of Alberta, Edmonton, Edmonton, Canada T6G 1Z2. E-mail: {ron.sloboda, nawaid.usmani}@albertahealthservices.ca.

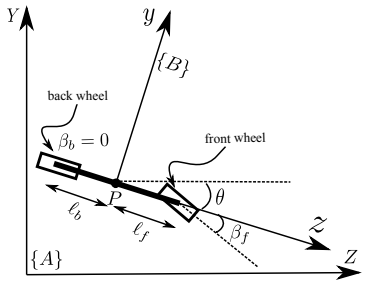

Fig. 1. General bicycle posture coordinates

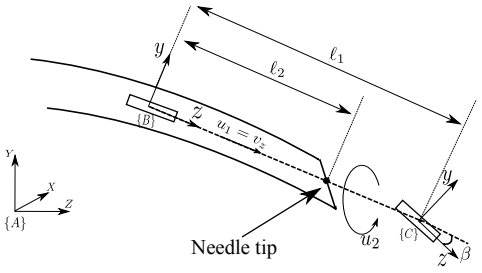

Fig. 2. Bicycle of a bevel tip needle

in Figure 1, the velocity components of wheel centers along the z and y axis can be expressed in frame $\{B\}$ as

$$^{B}v_{zi} = cos(\theta+\beta_i)\dot{z} + sin(\theta+\beta_i)\dot{y} + \ell_i sin\beta_i\dot{\theta} \quad (1)$$

$$^{B}v_{y_i} = sin(\theta+\beta_i)\dot{z} - cos(\theta+\beta_i)\dot{y} - \ell_i cos\beta_i\dot{\theta} \quad (2)$$

in which $i = f, b$ and $\begin{bmatrix} y & z & \theta \end{bmatrix}^T$ and $\begin{bmatrix} \dot{y} & \dot{z} & \dot{\theta} \end{bmatrix}^T$ represent the 3×1 posture vector of the bicycle and its time derivative in the fixed frame, respectively. The typical wheels used in a bicycle satisfy the pure rolling and non-slipping constraints. Rolling occurs on the wheel plane, thus

$$^{B}v_{zi} - \omega_{wi} = 0 \quad (3)$$

Also, there is no slipping orthogonal to wheel plane, thus

$$^{B}v_{y_i} = 0 \quad (4)$$

In (3), ω_{wi} is the rolling speed of the wheels.

Placing the moving frame $\{B\}$ at the center of the back wheel leads to $\ell_b = 0$. If the front wheel angle is constant, by redefining the bicycle parameters as $\ell_f = \ell$ and $\beta_1 = \beta$, the constraints (3) and (4) can be converted into the form of control system with the forward velocity input $u_1 = \omega_{wb}$ as

$$\begin{bmatrix} \dot{z} \\ \dot{y} \\ \dot{\theta} \end{bmatrix} = \begin{bmatrix} cos\theta \\ sin\theta \\ \ell(tan\beta)^{-1} \end{bmatrix} u_1. \quad (5)$$

Solving (5) for a constant forward velocity input u_1 results in the position of point P following a circle in $Y-Z$ plane with radius $\ell(tan\beta)^{-1}$.

B. Bicycle Model for Needle

A bevel tip needle inserted into soft tissue is usually driven with two inputs, namely longitudinal insertion and axial rotation. During insertion, as a result of tissue reaction forces, the needle bends in 3-D space. In [10], it is shown that the needle tip posture i.e., position and orientation, resembles the posture of a bicycle moving on circular planar path with the insertion velocity acting as the riding speed. Figure 2 illustrates this model of a bevel tip needle with the associated bicycle wheels. In this figure, frames $\{B\}$ and $\{C\}$ represent the moving body frames attached to the wheels. The parameters ℓ_1 and ℓ_2 denote the distance between the two wheels and the distance between the back wheel and the needle tip, respectively. In this model, the insertion velocity is equal to wheel rolling velocity v_z in the body frame $\{B\}$. Due to the planar motion of the bicycle, the velocity of frame $\{B\}$ along its x axis is zero. Writing in body frame this constraint can be expressed as

$$e_1^T v_{ab}^b = 0 \quad (6)$$

From (4) the velocity of frame $\{B\}$ does not have any projections along its y axis which can be written in the body frame as

$$e_2^T v_{ab}^b = 0 \quad (7)$$

Moreover, since the front wheel frame $\{C\}$ is rigidly connected to the back wheel frame the relative linear and angular velocity of the frame $\{C\}$ with respect to frame $\{B\}$ is zero. The velocity constraints of the body frame $\{C\}$ can be expressed in body frame as

$$e_1^T v_{ac}^b = e_2^T v_{ac}^b = 0 \quad (8)$$

in these equations v_{ab}^b and v_{ac}^b denote the linear velocity of the body frames $\{B\}$ and $\{C\}$ with respect to the fixed frame $\{A\}$ expressed in body frames, respectively and the vectors $e_i, i = 1, 2, 3$, represent the standard basis vectors in R^3. Equations (6)-(8) can be simplified to

$$\begin{bmatrix} 1 & 0 & 0 & 0 & 0 & 0 \\ 0 & 1 & 0 & 0 & 0 & \\ 0 & 0 & 1 & -\frac{1}{k} & 0 & 0 \\ 0 & 0 & 0 & 0 & 1 & 0 \end{bmatrix} V_{ab}^b = 0 \quad (9)$$

in which $k = \tan\beta{\ell_1}^{-1}$ denote the constant curvature of the needle tip path. $V_{ab}^b = \begin{bmatrix} v_{ab}^b & \omega_{ab}^b \end{bmatrix}^T$ is the 6-DOF representation of linear and angular velocities of the moving frame $\{B\}$. For $\ell_1 \neq 0$ and $\beta \in [0, \pi/2]$, solving for the null space of the matrix in (9) leads to the following kinematic model:

$$\dot{g}_{ab}(t) = g_{ab}(t)\left(u_1 \begin{bmatrix} e_3 \\ ke_1 \end{bmatrix} + u_2 \begin{bmatrix} 0 \\ e_3 \end{bmatrix}\right) \quad (10)$$

In (10), u_1 and u_2 denote the insertion velocity and the shaft rotation velocity, respectively, and g_{ab} is given by $g_{ab} = \begin{bmatrix} R_{ab} & p_{ab} \\ 0^T & 1 \end{bmatrix}$ with p_{ab} and R_{ab} being the position and orientation of the moving frame $\{B\}$ with respect to the fixed frame $\{A\}$.

III. Extended Bicycle model

In this section, we extend the bicycle model for a needle that follows a non-constant curvature path in tissue. The modified model incorporates new parameters to the bicycle's

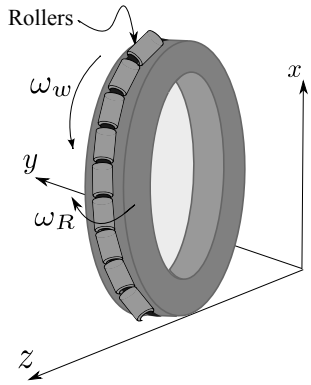

Fig. 3. An omni-directional wheel represents the bicycle's back wheel

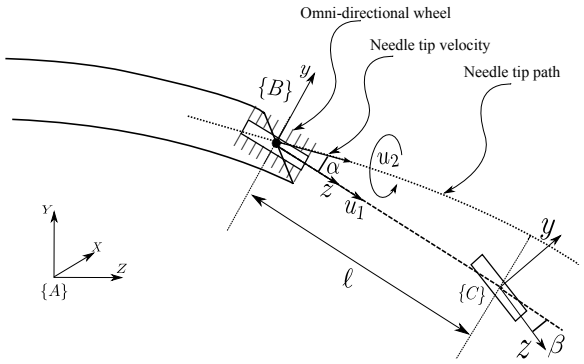

Fig. 4. Modified bicycle model of a bevel tip needle. The frames $\{C\}$ and $\{B\}$ are attached to front and back wheels. The back wheel is located at needle tip

kinematic equations to account for deviations of the needle path from a circle. The effect of tissue deformation can be interpreted as letting the needle have sideways movements orthogonal to the insertion direction. These movements are modeled by slippage of the bicycle wheels. As explained in the previous section, the original kinematic bicycle equations were derived by imposing the pure roll and non-slip constraints on the wheels.

In order to allow for sideways motion of the needle, we replace the back wheel of the bicycle with a wheel that is able to move in two directions. Omni-directional wheels shown in Figure 3 can move independently in two orthogonal directions. Such wheels satisfy the wheel plane constraint (3) but violate the non-slip constraint (4). Orthogonal to the wheel plane, the motion constraint will be

$$^{B}v_y - \omega_R = 0 \tag{11}$$

in which ω_R denotes the rotation velocity of the rollers. This is the degree of freedom added to the system allowing the wheel to have lateral movements.

Here, we replace the back wheel of the bicycle with the omni-directional wheel of Figure 3, as shown in Figure 4. In this Figure, β, ℓ and α denote the fixed front wheel angle, the distance between the two wheels and the rotation angle of the needle tip in body frame $\{B\}$, respectively. This rotation of the needle tip from the insertion direction by angle α is due to the lateral movement of the back wheel causing the needle to be tangent to the non-circular path. The inputs u_1 and u_2 denote the insertion velocity along the z axis of frame $\{B\}$ (which equals $^{B}v_z$) and the rotation velocity of the needle about its axis, respectively.

The lateral movements of the back wheel enables us to model the deviations of the needle tip trajectory from a circular path predicted by the conventional bicycle model. While the front wheel satisfies the pure rolling and non-slipping constraints of conventional wheels (3) and (4), the back wheel satisfies the roll and slip constraints (3) and (11). Therefore, the kinematic constraints on the front and back wheels are different.

The non-zero slip velocity is our modification to the conventional bicycle model. This value simulates the tissue deformation that deviates the needle tip position from a circular path. Since the amount of tissue compression depends on needle deflection, and the tip deflection and tip angle are related through trigonometric functions, we will consider $^{B}v_y$ as a function of needle tip angle. Moreover, the lateral movements can only happen when the needle is moving forward into tissue. In other words, when the insertion velocity $^{B}v_z$ is zero there will be no lateral movements. Accordingly, let us define the slippage equation of the back wheel as

$$^{B}v_y = f(\gamma, \lambda)^{B}v_z \tag{12}$$

in which λ is a tissue specific parameter (related to its mechanical properties) and f is an arbitrary function that we will define later that relates λ to the amount of lateral movements. The angle γ is the needle tip rotation in the fixed frame $\{A\}$ and is equal to $\theta + \alpha$. For a stiff tissue, λ equals zero and the needle tip travels on a circular path with $^{B}v_y = 0$, which implies $f(\theta, 0) = 0$. Using (12) and the constraints on the front and back wheels, the time variations of the back wheel angle is obtained as

$$\dot{\theta} = \frac{1}{l}[tan\beta + f(\gamma, \lambda)]^{B}v_z \tag{13}$$

The difference between (5) and (13) is that in (13), $\dot{\theta}$ is composed of two terms. The latter term represents the correction done to the original constant curvature solution using slippage of the back wheel. Using (12), the needle tip angle in body frame $\{B\}$ is found as

$$\alpha = tan^{-1}\left(\frac{^{B}v_y}{^{B}v_z}\right) = tan^{-1}(f(\gamma, \lambda)). \tag{14}$$

Using (12) and (14), the kinematics of the modified bicycle can be written as

$$\dot{y} = \left(\frac{sin\gamma}{cos\alpha}\right)^{B}v_z \tag{15}$$

$$\dot{z} = \left(\frac{cos\gamma}{cos\alpha}\right)^{B}v_z \tag{16}$$

$$\dot{\gamma} = \frac{\dot{\theta}}{1 - \partial\alpha/\partial\gamma} \tag{17}$$

in which $\partial\alpha/\partial\gamma$ is the partial derivative of α with respect to γ and $\dot{\theta}$ is defined in (13). Similar to equations (6) and (8), (15)-(17) can be written in the body frame $\{B\}$ as

$$e_1^T v_{ab}^b = 0 \tag{18}$$

$$e_2^T v_{ab}^b = f(\gamma,\lambda) e_3^T v_{ab}^b \tag{19}$$

$$e_1^T \omega_{ab}^b = \frac{1}{\ell}(tan\beta - f(\gamma,\lambda)) e_3^T v_{ab}^b \tag{20}$$

$$e_2^T \omega_{ab}^b = 0 \tag{21}$$

The equations (18)-(20) can be simplified to

$$\begin{bmatrix} 1 & 0 & 0 & 0 & 0 & 0 \\ 0 & 1 & -f(\gamma,\lambda) & 0 & 0 & 0 \\ 0 & 0 & 1 & -\frac{\ell}{\ell k - f(\gamma,\lambda)} & 0 & 0 \\ 0 & 0 & 0 & 0 & 1 & 0 \end{bmatrix} V_{ab}^b = 0 \tag{22}$$

in which $k = tan\beta\ell^{-1}$. As expected for $\lambda = 0$, (22) is equivalent to (9). Thus, the kinematic model (10) is found as $\dot{g}_{ab}(t) = g_{ab}(t)(u_1 V_1 + u_2 V_2)$ with $V_1 = \begin{bmatrix} 0 & f(\gamma,\lambda) & 1 & k - \frac{f(\gamma,\lambda)}{\ell} & 0 & 0 \end{bmatrix}^T$ and $V_2 = \begin{bmatrix} 0 & e_3^T \end{bmatrix}^T$.

A. Constraints on the Slippage Equation

In this section, we determine the constraints on the parameters of (12) for which the kinematics equations (15), (16), and (17) can be solved. Assuming that the needle tip angle relative to the fixed and the body frames take values in the range $[-\pi/2, \pi/2]$, the kinematic equations of the modified bicycle model can only be solved if the following conditions are satisfied:

$$cos(\alpha) \neq 0 \rightarrow \alpha \neq \pm\frac{\pi}{2} \tag{23}$$

$$1 - \frac{\partial\alpha}{\partial\gamma} \neq 0 \tag{24}$$

in which $\pm$ is selected depending on whether the needle tip points upward or downward.To derive these conditions and in order to keep the analysis traceable and avoiding complexities, the angle α that gives the slippage of the back wheel through (14) is defined as

$$\alpha = \lambda_1\gamma^2 + \lambda_2\gamma. \tag{25}$$

To simplify the equation, we will assume the needle path points toward the negative y axis and $\gamma, \alpha \in [-\pi/2, 0]$. In this case, (23) simplifies to

$$\lambda_1 > \frac{\lambda_2^2}{2\pi}. \tag{26}$$

Using this inequality, (24) can be written as

$$(1-\lambda_2) - 2\lambda_1\gamma > -\lambda_2^2\gamma/\pi + (1-\lambda_2). \tag{27}$$

For the right hand side of this inequality to be non-zero requires $\gamma > -\pi/4$, which for $\gamma \in [-\pi/2, 0]$ is acceptable and the right hand side will always be positive satisfying (24). From (26), if $\lambda_1 = 0$ then $\lambda_2 = 0$ and $\lambda_2 \neq 1$, which satisfies (24) for $\gamma = 0$. Although this condition seems to be restrictive, one can see that the absolute value of needle angle obtained from experiments for soft tissues is usually less than $\pi/4$. Figure 5 shows the needle path obtained by solving equations (15)-(17) numerically for different values of λ_1 and λ_2. As we can see for non-zero λ_1 and λ_2, the needle path deviates from the constant curvature circular path corresponding to $\lambda_1 = \lambda 2 = 0$.

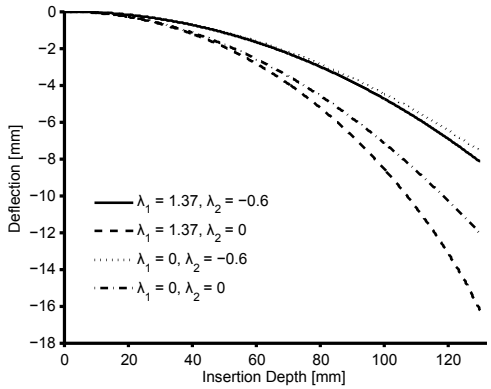

Fig. 5. Needle deflection calculated from extended model for different values of λ_1 and λ_2

IV. Experimental Verification

A. Experimental Setup

In order to study the effect of tissue stiffness on the needle path, experiments are performed on different types of tissues samples with different stiffnesses. The experimental setup used for conducting experiments is a 2-DOF prismatic-revolute robotic system shown in Figure 6. The base of the needle is connected to a step motor for axial needle rotation (not used in the experiments). The motor is assembled on a carriage for translational motion which is performed by another step motor through a belt and pulley mechanism. A webcam operating at 30 Hz is mounted above the tissue to capture images of the needle inside tissue and measure the needle deflection during insertion. The needle bevel angle is such that needle deflection happens in a plane parallel to the imaging plane. The detailed needle tip tracking procedure can be found in [11]. The needle used in the experiments is a standard 18 gauge brachytherapy needle with a bevel angle of 20°. The insertions are performed at different constant velocities to 130 mm insertion depth. Three trials are performed for each insertion velocity.

To assess the accuracy of the proposed model (15)-(17), the experiments are performed in two different transparent phantom tissues of two different types. The first tissue is made of plastisol gel (M-F Manufactoring Co., Fort Worth, USA) for which the amount of added plastic softener determines the stiffness of the tissue. The needle is inserted at 2 different velocities of 20 and 40 mm/sec. The second tissue is made of agar of type A360-500 (Fisher Scientific International Inc., Hampton, NH, USA) for which the ratio of agar to water used adjusts the stiffness of the tissue sample. The needle is inserted with constant insertion velocities of 20 and 60 mm/sec. In these experiments the insertion depth and needle tip deflection, are calculated from recorded images.

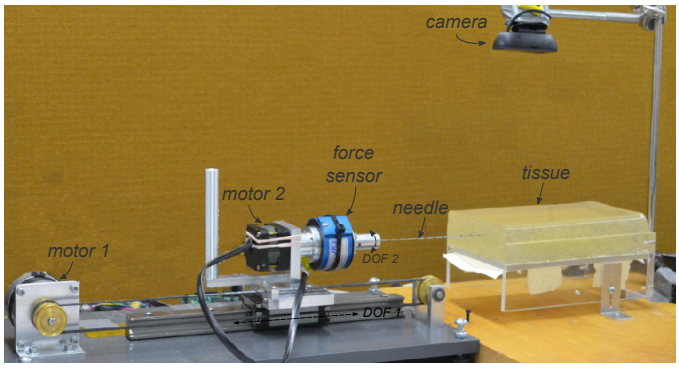

Fig. 6. Experimental setup used for collecting data. The needle is inserted into a phantom tissue using a 2-DOF prismatic-revolute robot. Images of the needle inside the tissue are recorded from above using a camera.

TABLE I

IDENTIFIED MODEL PARAMETERS AND MAXIMUM ERROR IN NEEDLE TIP ESTIMATION

Insertion parameters		Fitted model parameters		Maximum Error [mm]	
Tissue	Velocity [mm/sec]	λ_1	λ_2	Extended model	Bicycle model
Agar	20	0.49	0.22	**0.66**	3.79
	60			**0.33**	3.49
Plastisol	20	0.144	0.032	**0.43**	1.46
	40			**0.63**	0.76

From (25), the unknown constant parameters λ_1 and λ_2 are to be found by using experimental data. These parameters are found by fitting (17) to time variations of needle tip angle, $\dot{\gamma}$, calculated from the experimental data. To this end, third order time dependent polynomials are fitted to the depth and deflection data and the needle tip angle is approximated by

$$\gamma = sin^{-1}(\frac{\Delta y}{\Delta d}) \tag{28}$$

in which Δy and Δd denote the variations of the deflection and depth between two sample times, respectively. Using the approximated γ, its time variations is fitted to (17) using the `lsqcurvefit` function in Matlab. The obtained values for λ_1 and λ_2 are imported to the model equations (15), (16), (17) and the model is simulated for the same velocities as experiments.

For comparison, the experimental data is also fitted to standard bicycle model in which the needle path is estimated by a constant curvature path (circle). The results from both methods are shown in Figures 7 and 8. In these figures, the simulated deflection is compared to the average of three trials. For the agar tissue, the maximum prediction error obtained is 0.66 mm and 3.79 for the extended bicycle model and the original bicycle model, respectively. For plastisol tissue, the maximum prediction error is 0.43 mm and 1.46 mm for the extended bicycle model and the original bicycle model, respectively. The results are summarized in Table I. Comparing the maximum errors, we can conclude that for these combination of needle and tissue, the modified bicycle model generates smaller errors which is obtained by introducing new parameters to the kinematic equations of bicycle.

V. CONCLUSION

In this work, a modified kinematic bicycle model is developed for better estimating the needle tip deflection in soft tissue. The proposed model adds new parameters to the conventional bicycle model to account for the effect of tissue stiffness on the needle path. This alleviates the assumption made in the bicycle model that the tissue is stiff relative to needle. When this assumption is violated, however, the tissue compression forces caused by needle deflection deviate the needle path from a constant curvature path as predicted by the conventional bicycle model. To account for this, the back wheel of the bicycle is replaced with an omni-directional wheel enabling us to add correction terms to the bicycle equations. After fitting the experimental data to the model a maximum error of 0.66 mm in predicting the needle tip deflection is obtained, which is much smaller than 3.97 mm as the maximum error of the original bicycle model.

In this work, the modification to the bicycle model was done using polynomial functions in (25); however, it is possible to define other functions to relate the unknown parameters to physical properties of tissues. Besides, the experiments are performed for pure insertion case without any axial rotation of the needle. Further developments are required to verify the proposed model for case involving both insertion and rotation.

REFERENCES

[1] S. Misra, K. B. Reed, B. W. Schafer, K. Ramesh, and A. M. Okamura, "Mechanics of flexible needles robotically steered through soft tissue," *The International journal of robotics research*, 2010.

[2] N. V. Datla, B. Konh, M. Honarvar, T. K. Podder, A. P. Dicker, Y. Yu, and P. Hutapea, "A model to predict deflection of bevel-tipped active needle advancing in soft tissue," *Medical engineering & physics*, vol. 36, no. 3, pp. 285–293, 2014.

[3] E. Dehghan and S. E. Salcudean, "Needle insertion parameter optimization for brachytherapy," *Robotics, IEEE Transactions on*, vol. 25, no. 2, pp. 303–315, 2009.

[4] R. Alterovitz, K. Goldberg, and A. Okamura, "Planning for steerable bevel-tip needle insertion through 2d soft tissue with obstacles," in *Robotics and Automation, 2005. ICRA 2005. Proceedings of the 2005 IEEE International Conference on*. IEEE, 2005, pp. 1640–1645.

[5] S. P. DiMaio and S. E. Salcudean, "Needle insertion modeling and simulation," *Robotics and Automation, IEEE Transactions on*, vol. 19, no. 5, pp. 864–875, 2003.

[6] A. Boroomand, M. Tavakoli, R. Sloboda, and N. Usmani, "Dynamical modeling and controllability analysis of a flexible needle in soft tissue," *International Journal of Modeling, Simulation, and Scientific Computing*, vol. 5, no. 02, 2014.

[7] M. Khadem, B. Fallahi, C. Rossa, R. Sloboda, N. Usmani, and M. Tavakoli, "A mechanics-based model for simulation and control of flexible needle steering in soft tissue," in *Robotics and Automation, 2015. ICRA 2015. Proceedings of the 2015 IEEE International Conference on*. IEEE, 2015.

[8] W. Park, J. S. Kim, Y. Zhou, N. J. Cowan, A. M. Okamura, and G. S. Chirikjian, "Diffusion-based motion planning for a nonholonomic flexible needle model," in *Robotics and Automation, 2005. ICRA 2005. Proceedings of the 2005 IEEE International Conference on*. IEEE, 2005, pp. 4600–4605.

[9] D. C. Rucker, J. Das, H. B. Gilbert, P. J. Swaney, M. I. Miga, N. Sarkar, and R. J. Webster, "Sliding mode control of steerable needles," 2013.

[10] R. J. Webster, J. S. Kim, N. J. Cowan, G. S. Chirikjian, and A. M. Okamura, "Nonholonomic modeling of needle steering," *The International Journal of Robotics Research*, vol. 25, no. 5-6, pp. 509–525, 2006.

[11] T. Lehmann, M. Tavakoli, N. Usmani, and R. Sloboda, "Force-sensor-based estimation of needle tip deflection in brachytherapy," *Journal of Sensors*, vol. 2013, 2013.

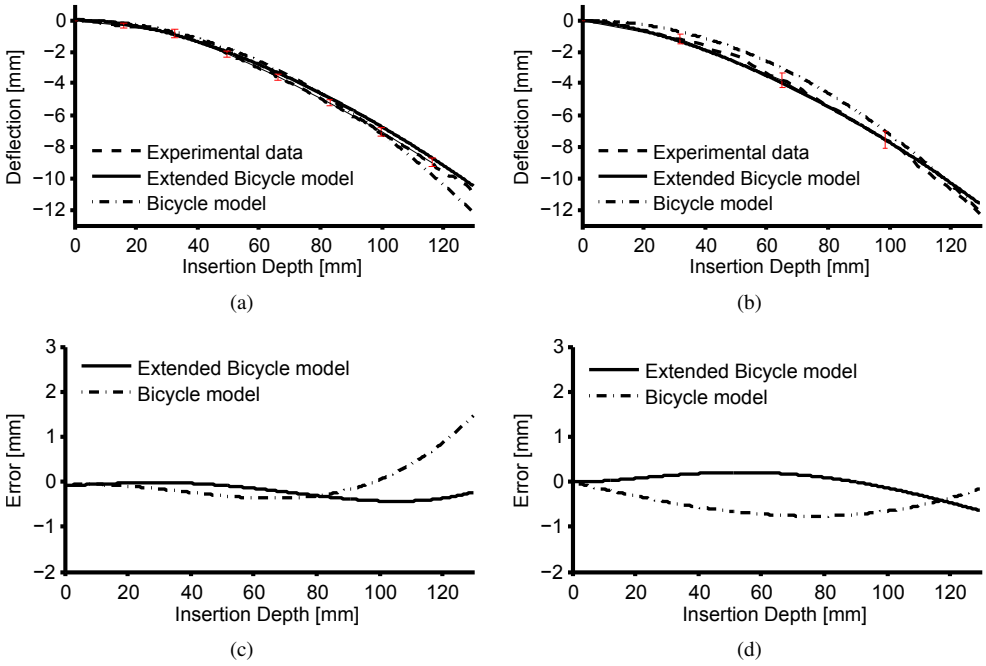

Fig. 7. Experimental results for needle insertion in plastisol tissue for different velocities. (a),(b): Needle deflection estimated from the modified bicycle model and the original bicycle model compared to experimental data for 20 mm/sec and 40 mm/sec, respectively (c),(d): Comparison of needle tip deflection estimation error for the modified bicycle model and the original bicycle model for 20 mm/sec and 40 mm/sec, respectively.

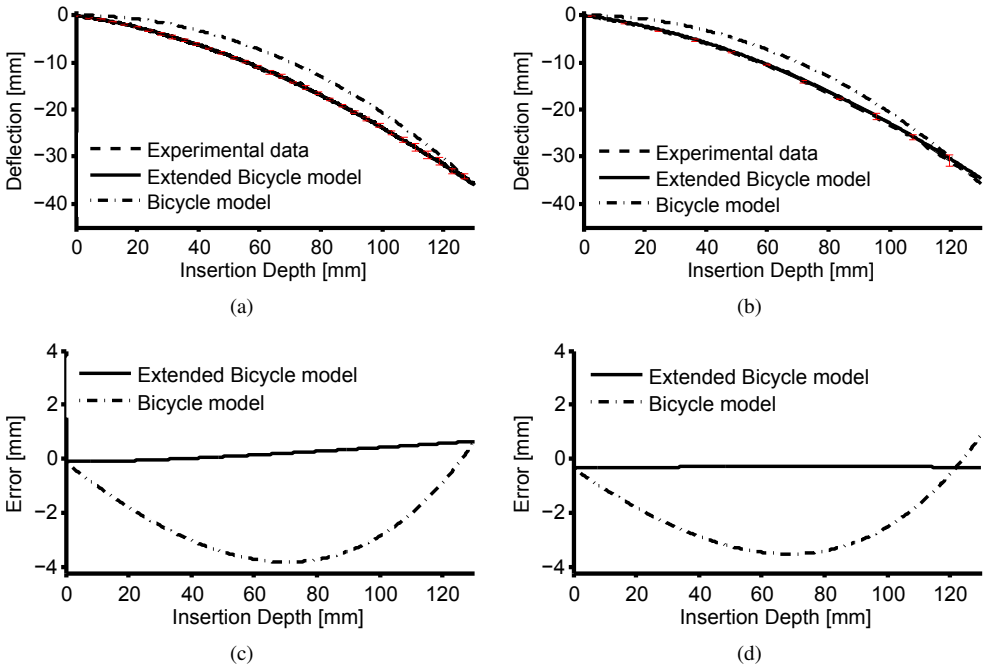

Fig. 8. Experimental results for needle insertion in agar tissue for different velocities. (a),(b): Needle deflection estimated from the modified bicycle model and the original bicycle model compared to experimental data for 20 mm/sec and 60 mm/sec, respectively (c),(d): Comparison of needle tip deflection estimation error for the modified bicycle model and the original bicycle model for 20 mm/sec and 60 mm/sec, respectively.